Spin dynamics and the Haldane gap in the spin-1 quasi-one-dimensional antiferromagnet $CsNiCl_3$

Rose M. Morra
Atomic Energy of Canada Limited, Chalk River, Ontario, Canada K0J 1J0
and Department of Physics, University of Toronto, Toronto, Ontario, Canada M5S 1A1

William J. L. Buyers
Atomic Energy of Canada Limited, Chalk River, Ontario, Canada K0J 1J0

Robin L. Armstrong
Atomic Energy of Canada Limited, Chalk River, Ontario, Canada K0J 1J0
and Department of Physics, University of Toronto, Toronto, Ontario, Canada M5S 1A1

K. Hirakawa
Institute for Solid State Physics, University of Tokyo, Tokyo 113, Japan
(Received 17 August 1987; revised manuscript received 22 February 1988)

A full description of a series of spin-wave measurements in $CsNiCl_3$ in the three-dimensional (3D) and one-dimensional (1D) phases and their analysis to provide the first experimental evidence for the Haldane gap is presented. Neutron scattering experiments were performed on a single crystal of $CsNiCl_3$ with both $(h,0,l)$ and (h,h,l) as the scattering plane. The order parameter in both 3D phases was measured and the spin-wave dispersion determined in the lower phase. The spin-wave spectrum calculated from a dynamic susceptibility method was compared with the experimental response in the lower 3D phase to obtain the following values for the exchange and anisotropy constants: $J=0.345\pm0.008$ THz, $J'=0.0060\pm0.005$ THz, and $D=-0.0130\pm0.0015$ THz. These parameters confirm that $CsNiCl_3$ in its disordered phase is a good approximation to a one-dimensional Heisenberg antiferromagnet. In the 1D phase the gap frequency for an isolated chain of Ni^{2+} ions is found to be 0.32 THz close to the gap estimated in finite-chain calculations. The results constitute experimental support for the Haldane conjecture that the excitations of integer-spin chains, unlike half-integer–spin chains, exhibit an apparent anisotropy that arises not from the underlying isotropic Hamiltonian, but from many-body effects.

I. INTRODUCTION

Haldane[1] has conjectured that integer-spin chains with isotropic coupling would have properties that are inherently different from those of half-integer–spin chains. He predicted that an integer-spin chain would exhibit a gap in its excitation spectrum, while all half-integer–spin chains would be gapless. This conjecture has stimulated considerable interest[2] and controversy.

Finite-size scaling methods have been used to determine the excitation spectrum of a spin-1 Heisenberg antiferromagnetic chain. Botet and Jullien[3] and Botet, Jullien, and Kolb[4] have estimated the size of the gap for a chain with Hamiltonian

$$H=\sum_i(\hat{S}_i^x\hat{S}_{i+1}^x+\hat{S}_i^y\hat{S}_{i+1}^y+\lambda\hat{S}_i^z\hat{S}_{i+1}^z)+D\sum_i(\hat{S}_i^z)^2 .$$

Their calculations are for finite rings of $N=4$, 6, 8, 10, and 12 spins using the Lanzcös algorithm; they then extrapolate their results to infinite N. The gap between the two lowest-lying states was nonzero, with a maximum value ~0.25 at the Heisenberg point $(D=0,\lambda=1)$. As a function of D, the gap decreased to zero near $D=1$ and $D>1$, the gap increased as D increased. Analytic solutions of the plane-rotation model $(D\geq0)$ have been obtained for spin 1 by Mattis[5] for a restricted set of parameters. The results are in agreement with the work of Botet, Jullien, and Kolb[4] but have not been obtained for the Heisenberg point.

Sólyom and Ziman[6] have argued that finite-lattice-extrapolation techniques lead to ambiguous results for the $S=1$ antiferromagnet chain at the Heisenberg point. Bonner and Muller[7] initially rejected the existence of the gap since a similar analysis for finite $S=\frac{1}{2}$ chains also appeared to predict a gap. However, Botet, Jullien, and Kolb[8] and Kolb, Botet, and Jullien[9] have shown some similarities in the convergence of finite-chain results to infinite N for $S=\frac{1}{2}$, $S=\frac{3}{2}$ chains, and differences between the convergence for these chains and the convergence for $S=1$ chains. More recent calculations using Lanzcös, Bethe Ansatz, and Monte Carlo techniques by Parkinson *et al.*[10] agree with those of Botet, Jullien, and Kolb[4] but predict an even larger gap of 0.40 at the Heisenberg point.

The first experimental evidence[11] for the Haldane gap was found in $CsNiCl_3$, a good example of a spin-1 one-dimensional antiferromagnet near the Heisenberg point. Here we present the full description of the spin waves and interaction parameters that underlie this earlier result. The second known example of the Haldane gap has been

reported[12] in the organic crystal $Ni(C_2H_8N_2)_2NO_2ClO_4$. The significance of our confirmation of the Haldane conjecture as an example of a general tendency for lowering of a classical symmetry in physical systems has been discussed[13] in terms of quantum effects creating a spin-wave mass.

The properties of $CsNiCl_3$ are summarized in Sec. II. The calculation of the spin-wave spectrum is discussed in Sec. III. The experimental results and their analysis are presented in Sec. IV for the three-dimensional (3D) phase and in Sec. V for the one-dimensional (1D) phase. Finally, in Sec. VI the results of this study are discussed in relation to other experimental work.

II. PROPERTIES OF $CsNiCl_3$

The 1D properties of $CsNiCl_3$ have been studied by several experimental techniques. Near 30 K, magnetic-susceptibility,[14] specific-heat,[15] and acoustic-attenuation[16] measurements all show a broad maximum characteristic of short-range 1D ordering. The spin-lattice relaxation rate for the ^{133}Cs nuclei[17] is dominated by diffusive behavior associated with spin fluctuations in isotropic chains. The elastic modulus C_{33} shows the effect of 1D spin-spin ordering near 30 K.[18]

The quasi-1D nature of the spin exchange in $CsNiCl_3$ may be understood by considering its crystallographic structure. The space group is D_{6h}^4 with lattice constants $a=7.14$ Å and $c=5.96$ Å. There are two formula units per unit cell. The coordinates for the two Ni^{2+} ions are (0,0,0), $(0,0,\frac{1}{2})$, for the six Cl^- ions are $\pm(x,2x,\frac{1}{4})$, $\pm(2\bar{x},\bar{x},\frac{1}{4})$, $\pm(x,\bar{x},\frac{1}{4})$ with $x=0.156$, and for the two Cs^+ ions, $\pm(\frac{2}{3},\frac{1}{3},\frac{1}{4})$. The Ni^{2+}-Cl^--Ni^{2+} superexchange path along the c axis results in a strong intrachain exchange coupling J, while the Ni^{2+}-Cl^--Cl^--Ni^{2+} path in the basal plane results in a weaker interchain coupling J'.

The lowest $3F$ term of a free Ni^{2+} ion in the approximately cubic octahedral field gives the ground orbital state $^3A_{2g}(S=1)$. This state is separated by about 8–10 000 cm^{-1} from the first triplet excited state. Because the orbital angular momentum of the ground state is quenched, the spin exchange between Ni^{2+} ions is of the isotropic Heisenberg form. The trigonal distortion and spin-orbit coupling should combine[11] to produce a planar single-site anisotropy, since the distortion from cubic is in the same sense as that for the strongly XY ferromagnet $CsNiF_3$. However, the susceptibility gives z as the easy axis so that the anisotropy has taken on Ising-like character. This is perhaps the earliest evidence for a Haldane gap effect. The spin Hamiltonian is therefore of the form

$$H=J\sum_{i,j}\mathbf{S}_i\cdot\mathbf{S}_j+J'\sum_{i,j}\mathbf{S}_i\cdot\mathbf{S}_j+D\sum_i(S_i^z)^2\ ,$$

where the first two sums are over nearest-neighbor pairs along the chain and in the basal plane, respectively. Since the exchange coupling is antiferromagnetic, $J,J'>0$; since the anisotropy of the susceptibility is easy axis, $D<0$. Estimates for the parameters[14,15,19–22] are listed in Table I.

Because of the weak-interchain exchange, $CsNiCl_3$ undergoes two magnetic phase transitions, at $T_{N1}=4.84$ K and $T_{N2}=4.40$ K as evidenced by NMR and specific-heat measurements.[23] The transitions are also seen in the elastic modulus C_{33} which has a small dip at 4.85 K and a sharp anomalous dip at 4.4 K.[18] Kadowaki, Ubukoshi, and Hirakawa[24] have shown that the upper transition corresponds to ordering of the z components of the moments and the lower to the additional ordering of the xy components. The magnetic structure below 4.4 K (Fig. 1) has been studied by neutron diffraction both on a powder sample[25] and on a single crystal.[26,27] The ordered spins lie in a plane which includes the c axis. On one-third of the chains, the spins are antiferromagnetically ordered and aligned along the c axis. The spins are also antiferromagnetically ordered along the other chains, but canted at an angle $\pm\theta$ away from the c axis. In the classical approximation, the energy per spin at 0 K

$$E=-\tfrac{1}{6}\{24J-2D-4D\cos^2\theta+24J'[2\cos\theta-\cos(2\theta)]\}S^2$$

is minimized to obtain the equilibrium condition for θ:

TABLE I. Estimates for the exchange and anisotropy parameters of $CsNiCl_3$.

J (THz)	D (THz)	J' (THz)	J'/J	Ref.
0.33	−0.12			12
0.28	−0.014			13
0.34	−0.008			17
	−0.015	0.042		18
			7×10^{-3}	19
	−0.002			20
0.345	−0.013	0.006	2×10^{-2}	This work

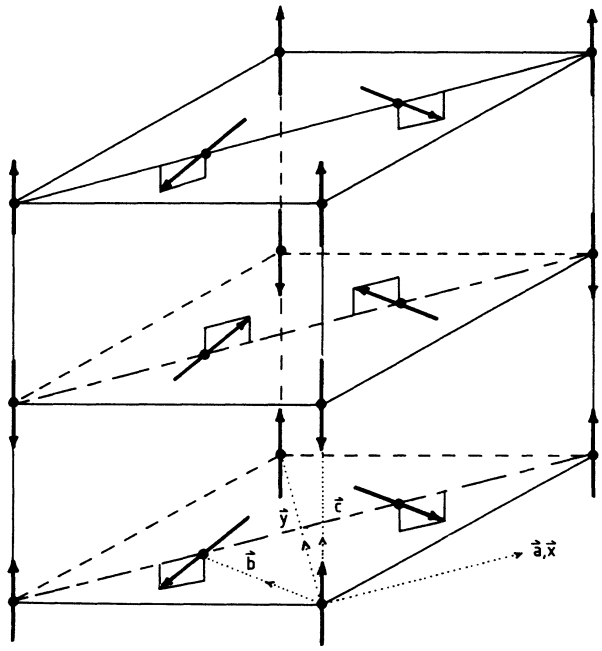

FIG. 1. Magnetic structure of $CsNiCl_3$ below 4.4 K shown for canting in the (x,y) plane.

$$\cos\theta=\begin{cases}\dfrac{1}{2(1+D/12J')}, & \text{for } -D<6J',\\ 1, & \text{for } -D\geq 6J'.\end{cases}$$

As the temperature was lowered, the angle θ was found to increase rapidly from $\sim 38°$ at 4.4 K and level off at 59° at 1.6 K. The moment for Ni^{2+} extrapolated to 0 K is $1.05\mu_B$ (Ref. 25) which is considerably smaller than the free-ion value $2\mu_B$ as discussed by Montano, Cohen, and Shechter.[19]

^{35}Cl and ^{133}Cs NMR measurements[19] in the intermediate phase of $CsNiCl_3$ show that there is no magnetic moment in the basal plane. This suggests that the structure is partially dynamic; that is, the longitudinal spin components are ordered as below 4.4 K but the transverse components are disordered. This is confirmed by the recent neutron measurements of Kadowaki, Ubukoshi, and Hirakawa.[24] The low-temperature coefficients of expansion support the partially dynamic model, since at 4.84 K, $\alpha_{\parallel}$ has a sharp maximum, and at 4.4 K, $\alpha_{\perp}$ has a sharp maximum, while $\alpha_{\parallel}$ has a small negative cusp.[28] The dynamic structure is also supported by specific-heat measurements which show spikes of approximately equal area at 4.4 and 4.85 K indicating that at each phase transition the number of magnetic degrees of freedom involved must be about the same.[29]

III. SPIN-WAVE SPECTRUM FOR THE CANTED STRUCTURE

The spin-wave spectrum in the low-temperature phase has been calculated from the dynamic susceptibility method of Buyers, Holden, and Perreault.[30] A molecular field calculation is first performed that gives the magnitude and canting angle of the spin at each of the $k=6$ sites in the antiferromagnetic unit cell. This calculation results in a set of single-ion states $|k,n\rangle$, $n=1,\ldots,2S+1$, with energies ω_{kn} and yields the matrix elements of the spin component in the α direction

$$S^{\alpha}_{kmn}=\langle k,m\,|\,S^{\alpha}(k)\,|\,k,n\rangle$$

in terms of which of the single-ion susceptibilities are

$$g^{\alpha\beta}_{k}(\omega)=\sum_{m,n}\frac{S^{\alpha}_{knm}S^{\beta}_{kmn}(f_{kn}-f_{km})}{\omega-\omega_{km}+\omega_{kn}},$$

where the fractional population of state $|k,n\rangle$ is the Boltzmann factor f_{kn}. Thus $g^{\alpha\beta}_{k}(\omega)$ contains the molecular exchange field and the anisotropy DS_z^2. The spin-wave frequencies and intensities are then given by the poles and residues of the dynamic susceptibility

$$G^{\alpha\beta}_{kk'}(\mathbf{Q},\omega)=g^{\alpha\beta}_{k}(\omega)\delta_{kk'}+2\sum_{k''}\sum_{\delta\gamma}g^{\alpha\delta}J^{\delta\gamma}_{kk'}(\mathbf{Q})G^{\gamma\beta}_{k''k'}(\mathbf{Q},\omega).$$

The neutron experiment at $T=0$ measures

$$S^{\alpha\beta}(\mathbf{Q},\omega)=-\pi^{-1}\mathrm{Im}\sum_{k,k'}G^{\alpha\beta}_{kk'}(\mathbf{Q},\omega).$$

The sublattice magnetizations are parametrized by the two variables S and θ such that for the spin at the origin $\mathbf{S}_1=S(0,0,1)$, for the spin at **a**, $\mathbf{S}_5=S(-\sin\theta,0,-\cos\theta)$, for the spin at 2**a**, $\mathbf{S}_3=S(\sin\theta,0,-\cos\theta)$, with spins 4, 2, and 6 in the adjacent plane at $\frac{1}{2}\mathbf{c}$ antiparallel to these. The nonzero intersublattice exchanges are

$$J(\mathbf{Q})=J^{\alpha\alpha}_{14}(\mathbf{Q})=J^{\alpha\alpha}_{25}(\mathbf{Q})=J^{\alpha\alpha}_{36}(\mathbf{Q})=2JS\cos(\pi Q_c),$$

$$J'(\mathbf{Q})=J^{\alpha\alpha}_{15}(\mathbf{Q})=J^{\alpha\alpha}_{26}(\mathbf{Q})=J^{\alpha\alpha}_{31}(\mathbf{Q})=J^{\alpha\alpha}_{42}(\mathbf{Q})=J^{\alpha\alpha}_{53}(\mathbf{Q})=J^{\alpha\alpha}_{64}(\mathbf{Q})=J'\{\exp(-2\pi Q_a i)+\exp(-2\pi Q_b i)+\exp[2\pi(Q_a+Q_b)i]\}$$

with $J^{\alpha\alpha}_{ji}(\mathbf{Q})=J^{\alpha\alpha}_{ij}(\mathbf{Q})^*$, for $\alpha=x,y,z$. At $T=0$, in the limit $D=0$, the canting angle θ becomes 60°, and the sublattice magnetizations are equivalent under rotations of 60° about the normal to the canting plane. In this limiting case, the generalized susceptibility can be solved analytically. Let R, S be the 18×18 matrices

$$\mathbf{R}=\mathrm{diag}(\mathbf{I}=\mathbf{T}^6,\mathbf{T},\mathbf{T}^2,\mathbf{T}^3,\mathbf{T}^4,\mathbf{T}^5),$$

$$\mathbf{S}=\frac{1}{\sqrt{6}}\begin{vmatrix}\mathbf{I} & \mathbf{I} & \mathbf{I} & \mathbf{I} & \mathbf{I} & \mathbf{I}\\ \mathbf{I} & s\mathbf{I} & s^2\mathbf{I} & -\mathbf{I} & -s\mathbf{I} & -s^2\mathbf{I}\\ \mathbf{I} & s^2\mathbf{I} & s\mathbf{I} & \mathbf{I} & s^2\mathbf{I} & s\mathbf{I}\\ \mathbf{I} & \mathbf{I} & \mathbf{I} & -\mathbf{I} & -\mathbf{I} & -\mathbf{I}\\ \mathbf{I} & s\mathbf{I} & s^2\mathbf{I} & \mathbf{I} & s\mathbf{I} & s^2\mathbf{I}\\ \mathbf{I} & s^2\mathbf{I} & s\mathbf{I} & -\mathbf{I} & -s^2\mathbf{I} & -s\mathbf{I}\end{vmatrix},$$

$$s=\exp(2\pi i/3),$$

where $\mathbf{I}$ is the 3×3 unit matrix and $\mathbf{T}$, the matrix which maps $\mathbf{S}_i$ onto $\mathbf{S}_{i+1}$, $i=1,2,\ldots,5$ and $\mathbf{S}_6$ onto $\mathbf{S}_1$, is

$$\mathbf{T}=\begin{vmatrix}\frac{1}{2} & 0 & \frac{\sqrt{3}}{2}\\ 0 & 1 & 0\\ -\frac{\sqrt{3}}{2} & 0 & \frac{1}{2}\end{vmatrix}.$$

Under the transformation $\mathbf{A}\rightarrow\mathbf{S}^{\dagger}\mathbf{R}^{\dagger}\mathbf{A}\mathbf{R}\mathbf{S}$, the 18×18 matrices $\mathbf{g}(\omega),\mathbf{J}(\mathbf{Q})$ are simultaneously block diagonalized such that

$$\mathbf{g}'(\omega)=\mathbf{S}^{\dagger}\mathbf{R}^{\dagger}\mathbf{g}(\omega)\mathbf{R}\mathbf{S}=\mathrm{diag}[\mathbf{g}_1(\omega),\mathbf{g}_1(\omega),\mathbf{g}_1(\omega),\mathbf{g}_1(\omega),\mathbf{g}_1(\omega),\mathbf{g}_1(\omega)],$$

$$\mathbf{S}^{\dagger}R^{\dagger}\mathbf{J}(\mathbf{Q})\mathbf{R}\mathbf{S}=\mathrm{diag}[\mathbf{J}_1(\mathbf{Q}),\mathbf{J}_2(\mathbf{Q}),\mathbf{J}_3(\mathbf{Q}),\mathbf{J}_4(\mathbf{Q}),\mathbf{J}_5(\mathbf{Q}),\mathbf{J}_6(\mathbf{Q})],$$

where the 3×3 matrices $\mathbf{g}_1(\omega),\mathbf{J}_i(\mathbf{Q})$ $(i=1,2,\ldots,6)$ are

$$\mathbf{g}_1(\omega)=\begin{bmatrix} \omega_0/(\omega^2-\omega_0^2) & i\omega/(\omega^2-\omega_0^2) & 0 \\ -i\omega/(\omega^2-\omega_0^2) & \omega_0/(\omega^2-\omega_0^2) & 0 \\ 0 & 0 & 0 \end{bmatrix},$$

$$\mathbf{J}_1(\mathbf{Q})=\mathbf{J}(\mathbf{Q})T^3+\mathbf{J}'(\mathbf{Q})T^4+J'(\mathbf{Q})^*T^2 ,$$

$$\mathbf{J}_2(\mathbf{Q})=\mathbf{J}(\mathbf{Q})T^3+\mathbf{J}'(\mathbf{Q})sT^4+J'(\mathbf{Q})^*s^2T^2 ,$$

$$\mathbf{J}_3(\mathbf{Q})=\mathbf{J}(\mathbf{Q})T^3+\mathbf{J}'(\mathbf{Q})s^2T^4+J'(\mathbf{Q})^*sT^2 ,$$

$$\mathbf{J}_4(\mathbf{Q})=-\mathbf{J}(\mathbf{Q})T^3+\mathbf{J}'(\mathbf{Q})T^4+J'(\mathbf{Q})^*T^2 ,$$

$$\mathbf{J}_5(\mathbf{Q})=-\mathbf{J}(\mathbf{Q})T^3+\mathbf{J}'(\mathbf{Q})sT^4+J'(\mathbf{Q})^*s^2T^2 ,$$

$$\mathbf{J}_6(\mathbf{Q})=-\mathbf{J}(\mathbf{Q})T^3+\mathbf{J}'(\mathbf{Q})s^2T^4+J'(\mathbf{Q})^*sT^2 ,$$

with $\omega_0=4JS+6J'S$. The generalized spin susceptibility in the mean-field approximation is $\mathbf{H}(\mathbf{Q},\omega)=\mathbf{I}-2\mathbf{g}(\omega)\mathbf{J}(\mathbf{Q})$. Under the same transformation

$$\mathbf{H}'(\mathbf{Q},\omega)=\mathbf{S}^\dagger\mathbf{R}^\dagger\mathbf{H}(\mathbf{Q},\omega)\mathbf{R}\mathbf{S}$$
$$=\mathrm{diag}\{[\mathbf{I}-2\mathbf{g}_1(\omega)\mathbf{J}_1(\mathbf{Q})],[I-2\mathbf{g}_1(\omega)\mathbf{J}_2(\mathbf{Q})],[\mathbf{I}-2\mathbf{g}_1(\omega)\mathbf{J}_3(\mathbf{Q})],[\mathbf{I}-2\mathbf{g}_1(\omega)\mathbf{J}_4(\mathbf{Q})],$$
$$[\mathbf{I}-2\mathbf{g}_1(\omega)\mathbf{J}_5(\mathbf{Q})],[\mathbf{I}-2\mathbf{g}_1(\omega)\mathbf{J}_6(\mathbf{Q})]\}$$

The spin-wave frequencies $\omega_i(\mathbf{Q})$ satisfy the equation

$$\det\{\mathbf{H}[\mathbf{Q},\omega_i(\mathbf{Q})]\}=0$$

or equivalently

$$\det[\mathbf{I}-2\mathbf{g}_1(\omega)\mathbf{J}_i(\mathbf{Q})] , \quad i=1,2,\ldots,6 .$$

If we define

$$f(Q_a,Q_b)=\cos(2\pi Q_a)+\cos(2\pi Q_b)+\cos[2\pi(Q_a+Q_b)] ,$$

$$u(\mathbf{Q})=\tfrac{1}{2}[\omega_0-2J(\mathbf{Q})-\mathbf{J}'(\mathbf{Q})-\mathbf{J}'^*(\mathbf{Q})]$$
$$=4\mathbf{J}\sin^2(Q_c\pi/2)+\mathbf{J}'[3-f(Q_a,Q_b)] ,$$

$$v(\mathbf{Q})=\tfrac{1}{2}[\omega_0+2\mathbf{J}(\mathbf{Q})+2\mathbf{J}'(\mathbf{Q})+2\mathbf{J}'^*(\mathbf{Q})]$$
$$=4\mathbf{J}\cos^2(Q_c\pi/2)+J'[3+2f(Q_a,Q_b)] ,$$

$$\mathbf{Q}_0=(\tfrac{1}{3},\tfrac{1}{3},1) , \quad \mathbf{Q}_1=(0,0,1) , \quad \mathbf{Q}_2=(\tfrac{1}{3},\tfrac{1}{3},0) ,$$

the spin wave branches are

$$\omega_1^2(\mathbf{Q})=4u(\mathbf{Q})v(\mathbf{Q}) ,$$

$$\omega_4^2(\mathbf{Q})=4u(\mathbf{Q}+\mathbf{Q}_0)v(\mathbf{Q}+\mathbf{Q}_0) ,$$

$$\omega_2^2(\mathbf{Q})=4u(\mathbf{Q}+\mathbf{Q}_1)v(\mathbf{Q}+\mathbf{Q}_1) ,$$

$$\omega_5^2(\mathbf{Q})=4u(\mathbf{Q}-\mathbf{Q}_2)v(\mathbf{Q}-\mathbf{Q}_2) ,$$

$$\omega_3^2(\mathbf{Q})=4u(\mathbf{Q}+\mathbf{Q}_2)v(\mathbf{Q}+\mathbf{Q}_2) ,$$

$$\omega_6^2(\mathbf{Q})=4u(\mathbf{Q}-\mathbf{Q}_0)v(\mathbf{Q}-\mathbf{Q}_0) .$$

This spectrum consisting of six branches is equivalent to that obtained by extending the first branch over the zone of the paramagnetic phase and folding it back into the zone of the ordered phase.

To obtain the intensities of the spin waves, one must sum

$$\mathbf{G}(\mathbf{Q},\omega)=\mathbf{R}\mathbf{S}\mathbf{H}'^{-1}(\mathbf{Q},\omega)\mathbf{g}'(\omega)\mathbf{S}^\dagger\mathbf{R}^\dagger$$

over the sublattice indices to obtain the generalized susceptibility:

$$\bar{\mathbf{G}}(\mathbf{Q},\omega)=36\begin{bmatrix} \tfrac{1}{4}(B_++B_-) & 0 & \dfrac{-i}{4}(B_+-B_-) \\ 0 & A & 0 \\ \dfrac{i}{4}(B_+-B_-) & 0 & \tfrac{1}{4}(B_++B_-) \end{bmatrix},$$

where

$$A=\frac{u(\mathbf{Q})}{\omega^2-4u(\mathbf{Q})v(\mathbf{Q})}=\frac{1}{4}\left[\frac{u(\mathbf{Q})}{v(\mathbf{Q})}\right]^{1/2}\left[\frac{1}{\omega-2\sqrt{u(\mathbf{Q})v(\mathbf{Q})}}-\frac{1}{\omega+2\sqrt{u(\mathbf{Q})v(\mathbf{Q})}}\right],$$

$$B_\pm=\frac{v(\mathbf{Q}\pm\mathbf{Q}_0)}{\omega^2-4u(\mathbf{Q}\pm\mathbf{Q}_0)v(\mathbf{Q}\pm\mathbf{Q}_0)}$$
$$=\frac{1}{4}\left[\frac{v(\mathbf{Q}\pm Q_0)}{u(\mathbf{Q}\pm\mathbf{Q}_0)}\right]^{1/2}\left[\frac{1}{\omega-2\sqrt{u(\mathbf{Q}\pm\mathbf{Q}_0)v(\mathbf{Q}\pm\mathbf{Q}_0)}}-\frac{1}{\omega+2\sqrt{u(\mathbf{Q}\pm\mathbf{Q}_0)v(\mathbf{Q}\pm\mathbf{Q}_0)}}\right].$$

From the generalized susceptibility, it is apparent that only three branches have nonzero intensity, so that the neutron spin-wave response is

$$S(\mathbf{Q},\omega)\alpha f^2(\mathbf{Q})(1-\hat{Q}_y^2)\left[\frac{u(\mathbf{Q})}{v(\mathbf{Q})}\right]^{1/2}\delta[\omega\mp\omega(\mathbf{Q})]$$
$$+\tfrac{1}{4}f^2(\mathbf{Q})(1+\hat{Q}_y^2)\left[\left[\frac{v(\mathbf{Q}+\mathbf{Q}_0)}{u(\mathbf{Q}+\mathbf{Q}_0)}\right]^{1/2}\delta[\omega\mp\omega(\mathbf{Q}+\mathbf{Q}_0)]\mp\left[\frac{v(\mathbf{Q}-\mathbf{Q}_0)}{u(\mathbf{Q}-\mathbf{Q}_0)}\right]^{1/2}\delta[\omega\mp\omega(\mathbf{Q}-\mathbf{Q}_0)]\right],$$

where $\omega^2(\mathbf{Q})=4u(\mathbf{Q})v(\mathbf{Q})$. For parameters $J=0.345$ THz, $J'=0.0060$ THz, $D=0$, the spin-wave frequencies for the six branches for symmetry directions $(0,0,1+\eta)$, $(\eta,\eta,1)$, $(\frac{1}{3},\frac{1}{3},1+\eta)$ are shown in Fig. 2 and for directions $(\eta,0,1)$ and $(\eta+\frac{1}{2},0,\frac{1}{2})$ in Fig. 3. The relative intensities are indicated.

The response for the canted structure in the limit of zero anisotropy is formally identical to that for an antiferromagnet ABX_3 with easy plane anisotropy in which the spins order in the (x,y) plane at **O**, $\mathbf{S}_1=S(1,0,0)$; at **a**, $\mathbf{S}_2=S(-\frac{1}{2},\sqrt{3}/2,0)$; at 2**a**, $\mathbf{S}_3=S(\frac{1}{2},-\sqrt{3}/2,0)$, with antiferromagnetic ordering in the c direction. The calculated spin-wave response[24,31] also yields three branches of nonzero intensity. Although the anisotropy is believed to be very small[24] it will become clear that the model with $D=0$ cannot describe the data if only linear spin-wave theory is used.

For nonzero anisotropy, the spectrum for the canted structure has been calculated numerically for several values of J,J',D. Since only $T=0$ excitations are of interest, the temperature was set to 1 K, for which populations of excited molecular field states are negligible. For each of the six sublattices the mean-field Hamiltonian was diagonalized to obtain the molecular states and frequencies. The mean-field solution was found to be self-consistent for the canting angle θ given by $\cos\theta=[2(1+D/12J')]^{-1}$ for $-D<6J'$ and was unstable for $-D\geq 6J'$ and for $D>0$.

The frequencies of the branches $\omega_i(\mathbf{Q})$ were found by scanning $\det[\mathbf{H}(\mathbf{Q},\omega)]$ for zeroes as a function of frequency and refined to an accuracy of 0.0005 THz. The intensity of the spin wave was the residue of the 3×3 matrix $\mathbf{G}(\mathbf{Q},\omega_i(\mathbf{Q})+i\epsilon)$ for each of the polarizations xx, xz, zz, and yy. The y modes do not couple to the xz modes.

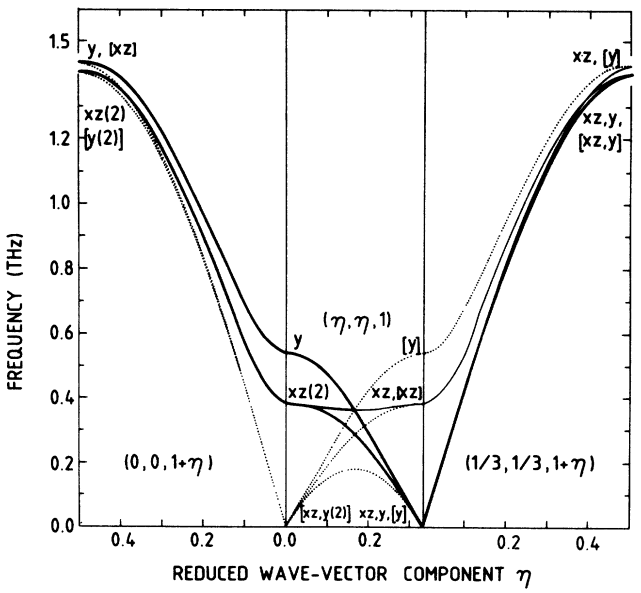

FIG. 2. Spin-wave spectrum for the canted structure with $J=0.345$ THz, $J'=0.0060$ THz, $D=0$ along symmetry directions $(0,0,1+\eta)$, $(\eta,\eta,1)$, $(\frac{1}{3},\frac{1}{3},1+\eta)$. Branches of strong intensity are indicated by dark lines, branches of weak intensity by medium lines, and branches of no intensity by dotted lines. Polarizations along x,y,z directions or in the (x,z) plane are also indicated.

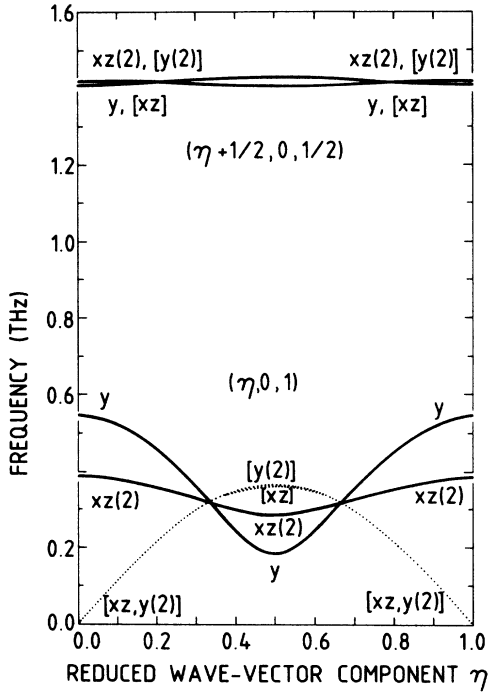

FIG. 3. Spin-wave spectrum for the canted structure with $J=0.345$ THz, $J'=0.0060$ THz, $D=0$ along symmetry directions $(\eta+\frac{1}{2},0,\frac{1}{2})$, $(\eta,0,1)$. The line codes and polarization designations are as in Fig. 2.

The numerical calculation was checked in the $D=0$ limit and the results found to agree with the analytical result. The spin-wave frequencies also agreed with a previous study[20] where the parameters $J=0.300$ THz, $J'=0.019$ THz, and $D=-0.015$ THz were used with the

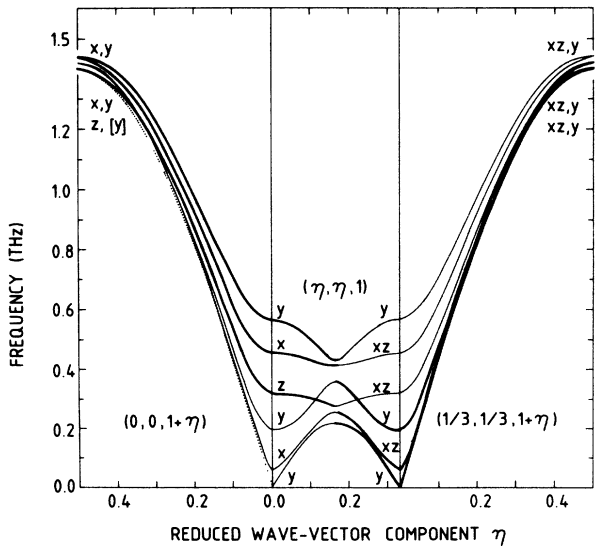

FIG. 4. Spin-wave spectrum for the canted structure with $J=0.345$ THz, $J'=0.0060$ THz, $D=-0.0130$ THz along symmetry directions $(0,0,1+\eta)$, $(\eta,\eta,1)$, $(\frac{1}{3},\frac{1}{3},1+\eta)$. The line codes and polarization designations are as in Fig. 2.

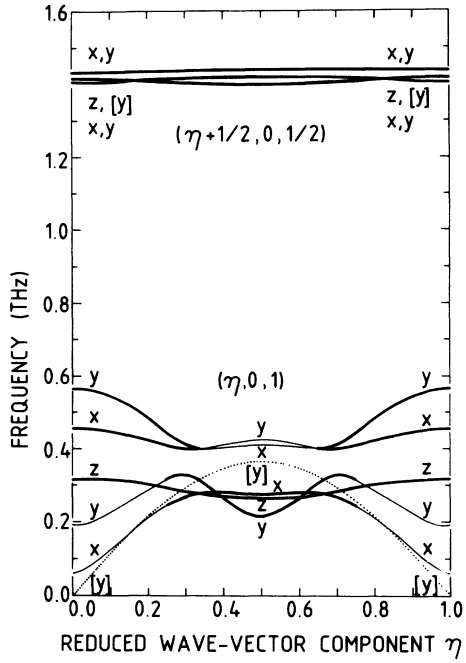

FIG. 5. Spin-wave spectrum for the canted structure with $J=0.345$ THz, $J'=0.0060$ THz, $D=-0.0130$ THz along symmetry directions $(\eta+\frac{1}{2},0,\frac{1}{2})$, $(\eta,0,1)$. The line codes and polarization designations are as in Fig. 2.

matching of matrix elements method. The spin-wave dispersion for the parameters that describe our experimental results $J=0.345$ THz, $J'=0.0060$ THz, and $D=-0.0130$ THz is shown in Figs. 4 and 5. Unlike the spectrum for $D=0$ (Figs. 2 and 3), the six branches are now, in general, nondegenerate and of finite intensity, although some branches are weak. For example, at (0,0,1), only three modes, one longitudinal and two transverse, have strong intensities. Of the three modes that have strong intensity at $(\frac{1}{3},\frac{1}{3},1)$, one is a Goldstone mode, one of very low frequency and one a finite-gap mode whose frequency is given by $\sqrt{\alpha J\,|\,D\,|}$, $8<\alpha<9$, where α is very close to the value 8 expected in the absence of interchain coupling. This shows that the gap depends only weakly on J. The Goldstone mode exists because there is no interaction in the Hamiltonian that gives preference to a particular direction in the basal plane for the perpendicular spin components.

IV. SPIN DYNAMICS IN THE THREE-DIMENSIONAL PHASE

Neutron-scattering experiments were performed on a single crystal of $CsNiCl_3$ with a mosaic spread of 0.35° using triple-axis spectrometers at the NRU reactor, Chalk River. The crystal was mounted in a temperature-variable cryostat with $(h,0,l)$ as the scattering plane in one experiment and (h,h,l) as the scattering plane for two additional experiments. The spectrometer configurations are given in Table II. The typical frequency resolution was 0.13 THz. The hexagonal lattice constants determined at 2.5 K were $a=7.09$ Å, $c=5.88$ Å. The temperature dependence of the intensity of the magnetic peak $(\frac{1}{3},\frac{1}{3},1)$ measured from 3.5 to 5.8 K indicates that there are two phase transitions at $T_{N1}=4.83\pm0.08$ K and $T_{N2}=4.46\pm0.08$ K, agreeing well with the transition temperatures determined from NMR and specific-heat data.[23] The Bragg peak relative intensities for $\eta=\frac{1}{3}$, $\frac{2}{3}$, $\frac{4}{3}$, and $\frac{5}{3}$ are plotted as a function of temperature in Fig. 6. Note that the greater strength of the anomaly at T_{N2} for small η, $(\frac{1}{3},\frac{1}{3},1)$ and $(\frac{2}{3},\frac{2}{3},1)$, is consistent with this transition involving y ordering. This corresponds to a freezing in of the rotation of the chirally ordered spin structure about the z axis. The upper transition at T_{N1} corresponds to the freezing in of the rotation in the (x,z) plane. These results are consistent with the structure proposed by Kadowaki, Ubukoshi, and Hirakawa[24] and with the theory of Xiaodong Zhu and Walker.[32]

To determine the spin-wave dispersion in the lower magnetic phase constant-Q measurements were made in both scattering planes. In the $(h,0,l)$ plane, measurements were made at $T=2.1$ K with fixed scattered neutron energy E_1 along the symmetry directions $(0,0,1+\eta)$, $(1,0,1+\eta)$, and $(\eta+\frac{1}{2},0,\frac{1}{2})$ using $E_1=3.3$ THz and along $(\eta,0,1)$ with a slightly lower E_1(2.0–3.0 THz). Only one peak was observed, with a maximum frequency of 1.52 ± 0.02 THz at $(0,0,1\frac{1}{2})$. Along $(0,0,1+\eta)$ the frequency decreased and the intensity of the peak increased as η decreased until at (0,0,1) the measured frequency was 0.52 ± 0.02 THz. Along $(\eta,0,1)$, the frequency continued to fall as the intensity increased to a minimum frequency 0.20 ± 0.01 THz at $(\frac{1}{2},0,1)$. Along $(\eta,0,\frac{1}{2})$, the peak was broad and weak with no dispersion. At $(\frac{1}{2},0,\frac{1}{2})$ the frequency of the peak was 1.39 ± 0.03 THz and its intensity was comparable to that of the peak at $(0,0,1\frac{1}{2})$.

Constant-Q measurements in the (h,h,l) plane were

TABLE II. Spectrometer configurations for experiments.

Experiment	1	2	3
Scattering plane	$(h,0,l)$	(h,h,l)	(h,h,l)
Monochromator	Si(1,1,1)	Si(1,1,1)	Si(1,1,1)
Mosaic spread	0.26°	0.24°	0.24°
Analyzer	PG[a](0,0,2)	Si(1,1,1)	Si(1,1,1)
Mosaic spread	0.35°	0.19°	0.19°[a]
Collimation before specimen	0.6°	0.4°	0.4°
Collimation after specimen	0.6°	0.8°	0.6°
Typical E_1	3.3 THz	2.5 THz	2.5 THz

[a]PG: Pyrolytic graphite.

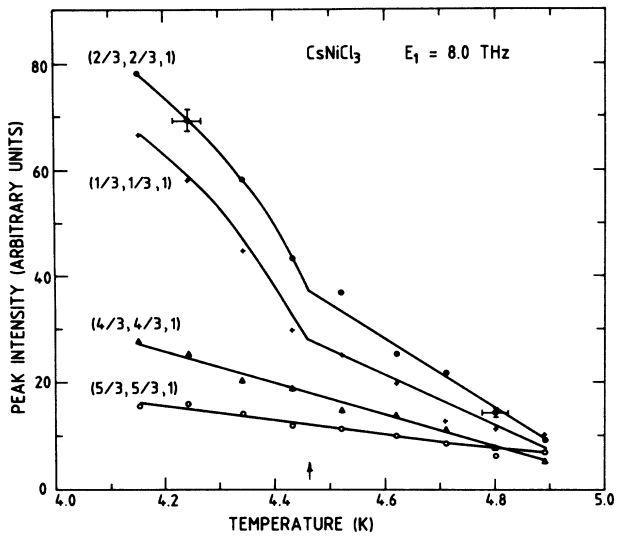

FIG. 6. Relative Bragg peak intensities for $\eta=\frac{1}{3}, \frac{2}{3}, \frac{4}{3}$, and $\frac{5}{3}$ as a function of temperature.

made along the $(\eta,\eta,1)$ and $(\frac{1}{3},\frac{1}{3},1+\eta)$ direction with $E_1=2.5$ THz, at or below 2.7 K. The single peak observed at (0,0,1) continued to fall in frequency and increase in intensity along $(\eta,\eta,1)$ until at (0.25,0.25,1) two overlapping peaks were discernible and at (0.28,0.28,1) the peaks were well separated in frequency. The lower peak was more intense and tended towards zero frequency while the upper peak had a finite frequency 0.19 ± 0.01 THz at $(\frac{1}{3},\frac{1}{3},1)$. Along $(\frac{1}{3},\frac{1}{3},1+\eta)$ two peaks were evident at $\eta=0.015$ and 0.03 but by $\eta=0.08$ only one peak could be seen. The peaks rose in frequency to 1.42 ± 0.02 THz at $(\frac{1}{3},\frac{1}{3},1\frac{1}{2})$ as the intensity continually decreased. Examples of the raw data are shown in Figs. 7 and 8. The frequencies calculated using the linear spin-wave model are indicated by arrows in Fig. 8.

To compare the theoretical spin-wave response with experiment, the calculated spectrum of Fig. 4 has been convoluted with the spectrometer frequency resolution, resulting in only one peak for all symmetry directions except near $(\frac{1}{3},\frac{1}{3},1)$, where two peaks, one of zero peak fre-

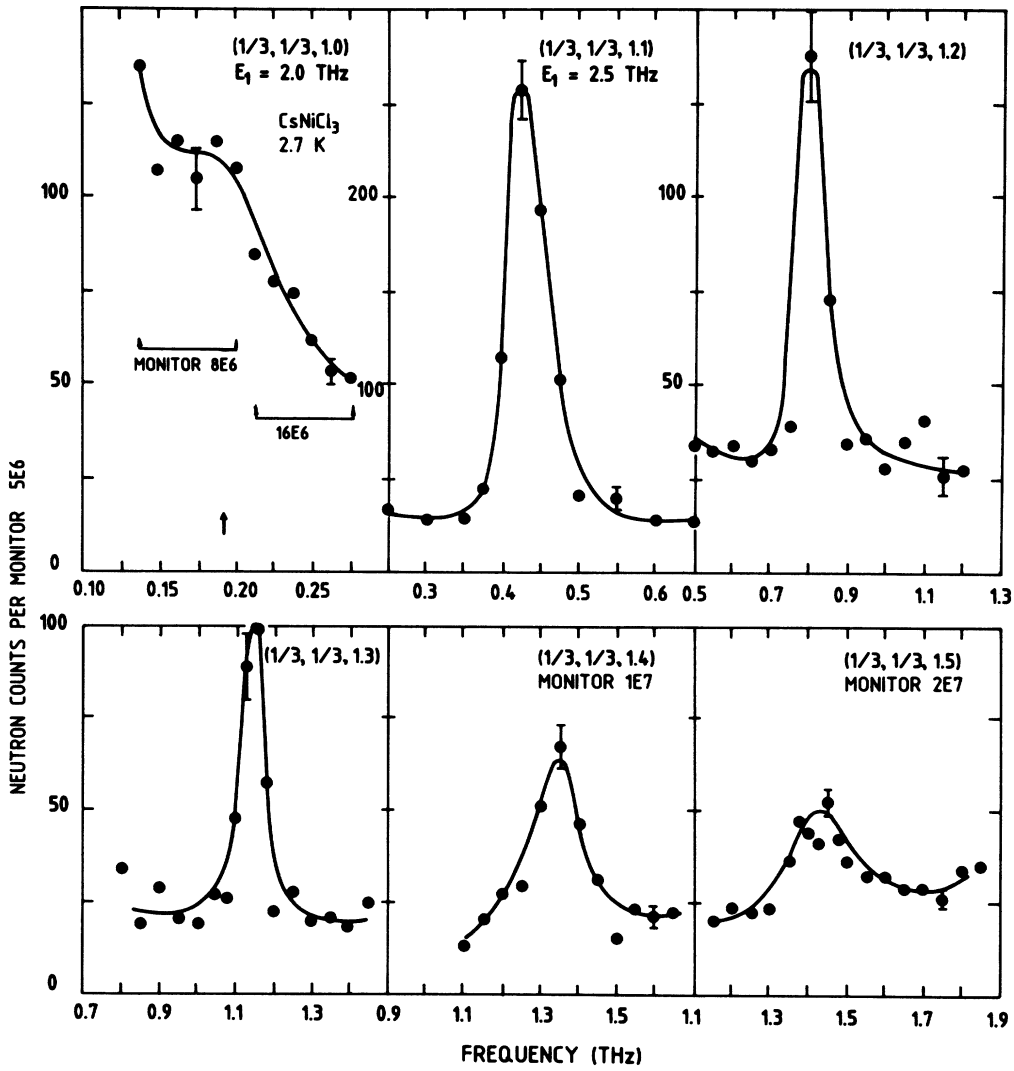

FIG. 7. Constant-Q scans in the three-dimensional phase along $(\frac{1}{3},\frac{1}{3},1+\eta)$. The monitor count, wave vector, final neutron energy E_1, and temperature for each constant-Q scan are indicated. In this and subsequent figures where the original data have been collected at a higher monitor this fact is indicated by a bracketed region.

quency, the other with a finite frequency, result. The response was then averaged over three wave-vector domains. The peak frequencies observed at (0,0,1), 0.52±0.02 THz; $(\frac{1}{3},\frac{1}{3},1)$, 0.19±0.01 THz; and $(\frac{1}{3},\frac{1}{3},1\frac{1}{2})$, 1.42±0.03 THz, are necessary and sufficient to determine the three parameters J, J', and D. By fitting to the peak frequencies at these three wave vectors, the following values for the exchange and anisotropy constants were obtained: $J=0.345\pm0.008$ THz, $J'=0.0060\pm0.0005$ THz, and $D=-0.0130\pm0.0015$ THz. The resulting peak frequencies of the averaged, convoluted response for these parameters are compared with the neutron-scattering spin-wave peaks in Fig. 9 for symmetry directions $(0,0,1+\eta)$, $(\eta,\eta,1)$, $(\frac{1}{3},\frac{1}{3},1+\eta)$, in Fig. 10 for $(\eta,0,1)$, $(\eta+\frac{1}{2},0,\frac{1}{2})$, and in Fig. 11 for $(1,0,1+\eta)$, $(1+\eta,0,1)$. It is evident that the model gives a good description of the spin waves, although at $(0,0,1\frac{1}{2})$ the predicted peak frequency is too low and at $(\frac{1}{2},0,1)$ it is

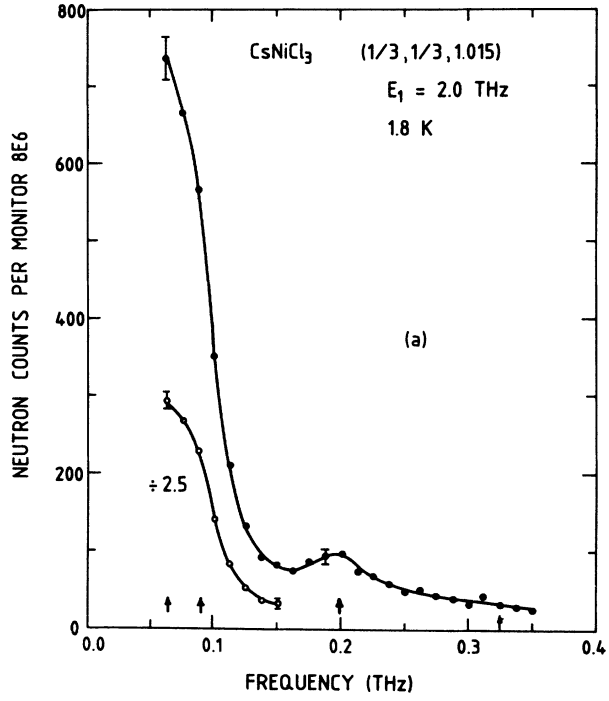

FIG. 8. Constant-Q scans in the three-dimensional phase at (a) $(\frac{1}{3},\frac{1}{3},1.015)$ and (b) $(\frac{1}{3},\frac{1}{3},1.03)$. The arrows indicate the frequencies calculated by the linear spin-wave model.

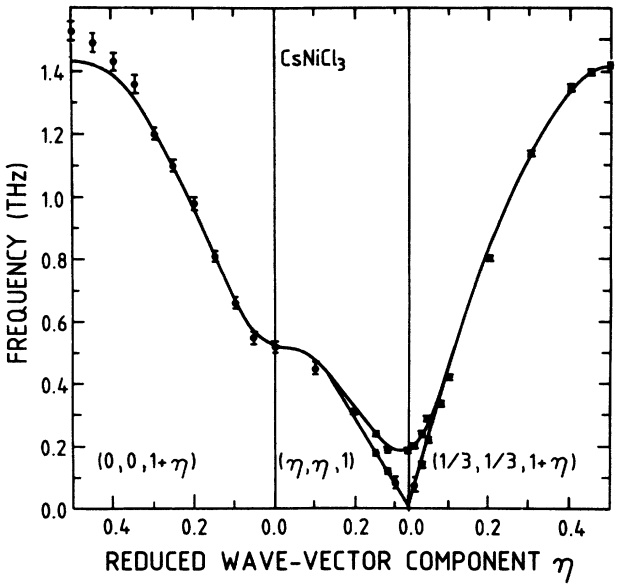

FIG. 9. Comparison of the calculated and observed spin-wave peak frequencies along symmetry directions $(0,0,1+\eta)$, $(\eta,\eta,1)$, $(\frac{1}{3},\frac{1}{3},1+\eta)$ in the three-dimensional phase.

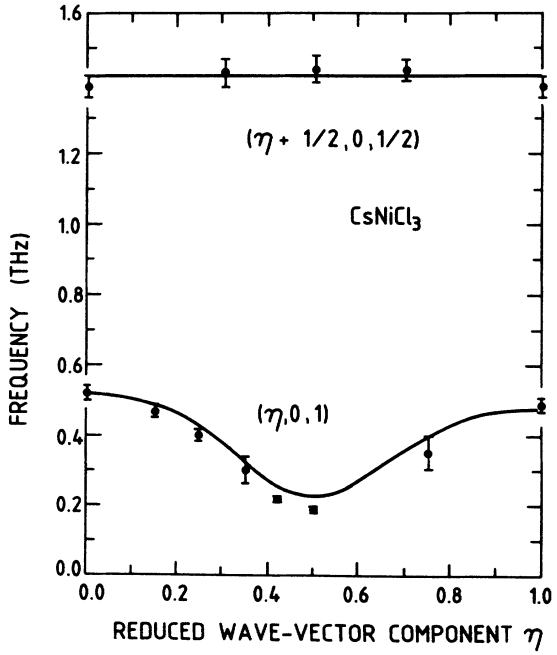

FIG. 10. Comparison of the calculated and observed spin-wave peak frequencies along symmetry directions $(\eta,0,1)$, $(\eta+\frac{1}{2},0,\frac{1}{2})$ in the three-dimensional phase.

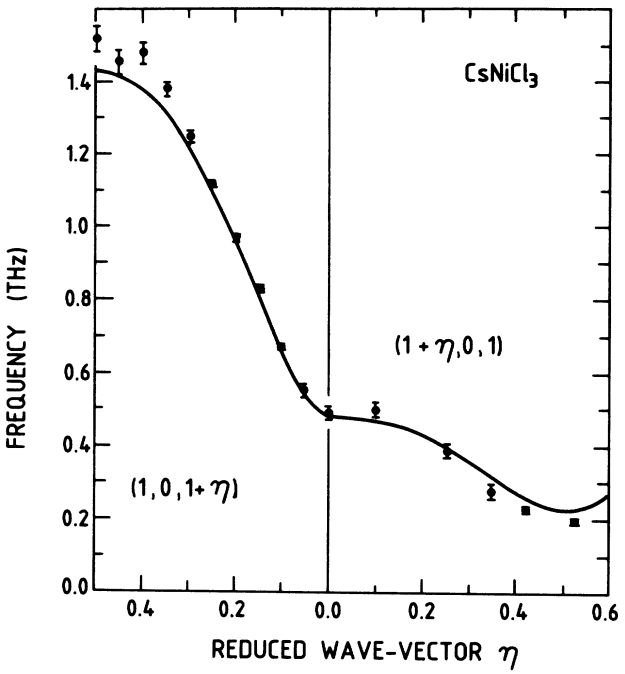

FIG. 11. Comparison of the calculated and observed spin-wave peak frequencies along symmetry directions $(1,0,1+\eta)$, $(1+\eta,0,1)$ in the three-dimensional phase.

too high. The fit is particularly good near $(\frac{1}{3},\frac{1}{3},1)$, where the two branches, one a Goldstone branch and the other a finite-gap branch, are fitted very well. The intensities of the peaks obtained from the convoluted and averaged spectrum agreed qualitatively with the intensities of the measured peaks.

Polarized neutron measurements by Steiner *et al.*[33] in a field perpendicular to the $(h,0,l)$ plane have confirmed that the lowest mode near $(\frac{1}{3},\frac{1}{3},1)$ is of the y symmetry predicted for the Goldstone mode by our theory (Fig. 4). However, the upper mode near 0.2 THz is found in the polarized measurements to be of xz symmetry. The parameters of the linear spin-wave model were systematically varied in order to obtain the correct polarization, but it was found that the model could not then reproduce the observed frequencies nor the correct canted structure. This shows that a linear spin-wave model that gives the correct canting angle and frequencies cannot give correct eigenvectors. The results of Kadawaki, Ubukoshi, and Hirakawa[24] suggest that it is likely that at T_{N1} an xz mode goes soft while at T_{N2} a y mode goes soft as found experimentally by Steiner *et al.*[33]

V. INVESTIGATION OF THE HALDANE CONJECTURE

To test the conjecture of the existence of a finite gap in the spectrum of a spin-1 antiferromagnetic Heisenberg chain, the spin-wave dispersion $CsNiCl_3$ above 4.8 K in the (h,h,l) plane was also investigated.[11] Constant-Q scans were made at several temperatures for $\mathbf{Q}=(0,0,1)$ and $\mathbf{Q}=(0.2,0.2,1)$ (Fig. 12). As the temperature increases, the spin-wave peaks at both wave vectors remain constant in frequency while decreasing slightly in intensity until at 17 K only a very broad and shallow peak remains at (0,0,1). To investigate the spin-wave dispersion in the 1D phase more closely, several of the constant-Q scans along $(\eta,\eta,1)$ and $(\frac{1}{3},\frac{1}{3},1+\eta)$ were repeated at 10 K. The most dramatic effect of the increase in temperature is seen near $(\frac{1}{3},\frac{1}{3},1)$. At (0.25,0.25,1) and (0.28,0.28,1) (Fig. 13) the two peaks of the lower magnetic phase are replaced by one broad peak with a significant decrease in intensity. Elsewhere the peak frequencies do not change while the intensity decreases along $(\frac{1}{3},\frac{1}{3},1+\eta)$ (Fig. 14). It is surprising that the high-frequency short-wavelength spin waves are so heavily damped above T_{N1}, whereas the low-frequency spin waves, although weakened, remain well defined. If the spectral weight of the latter (left-hand panel of Fig. 5) were spread over a similar large range ($\sim$0.5 THz) as the high-frequency excitations, the response would reach to zero frequency near the zone center. Thus it appears as if there is a minimum energy required to create an excitation.

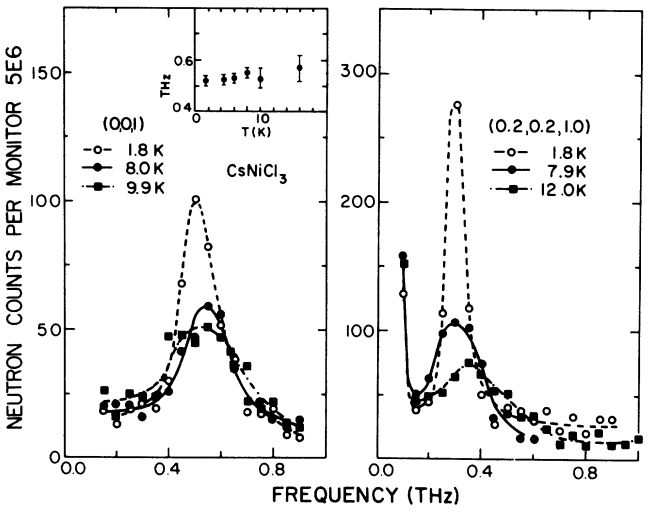

FIG. 12. Constant-Q scans at (0,0,1) and (0.2,0.2,1) at several temperatures. The inset indicates that the peak frequency for $\mathbf{Q}=(0,0,1)$ is temperature independent.

Along $(\eta,\eta,1)$ and $(\frac{1}{3},\frac{1}{3},1+\eta)$ a peak is obtained at a finite frequency without any measurable central mode intensity. From the constant-Q measurements along $(\eta,\eta,1)$ it is evident that basal plane dispersion, caused by interchain coupling, exists above $T_{N2}=4.84$ K. This dispersion is very surprising because 1D correlations predominate. The temperature is more than twice either Néel temperature and so is outside the critical region $\sim T_{N1}/z$ with $z=6$, expected for normal 3D short-range order. The strong anisotropy of the coupling, however, changes the concept of a critical region. It is possible to understand the dispersion if a gap exists in the spectrum of an isolated chain, at frequency ω_0, say. This gap corresponds to wave vector $\mathbf{Q}_c=(0,0,1)$, that is, the antiferromagnetic 1D zone center. Suppose the low-frequency response of each chain is described by a transverse susceptibility

$$g(\omega)=A/(\omega^2-\omega_0^2)\ .$$

Then an assembly of such chains weakly coupled above T_{N1} by an effective interchain exchange $\tilde{J}'$ will have a response

$$G(\mathbf{q}_b,\omega)=\frac{g(\omega)}{1-\tilde{J}'(\mathbf{q}_b)g(\omega)}$$

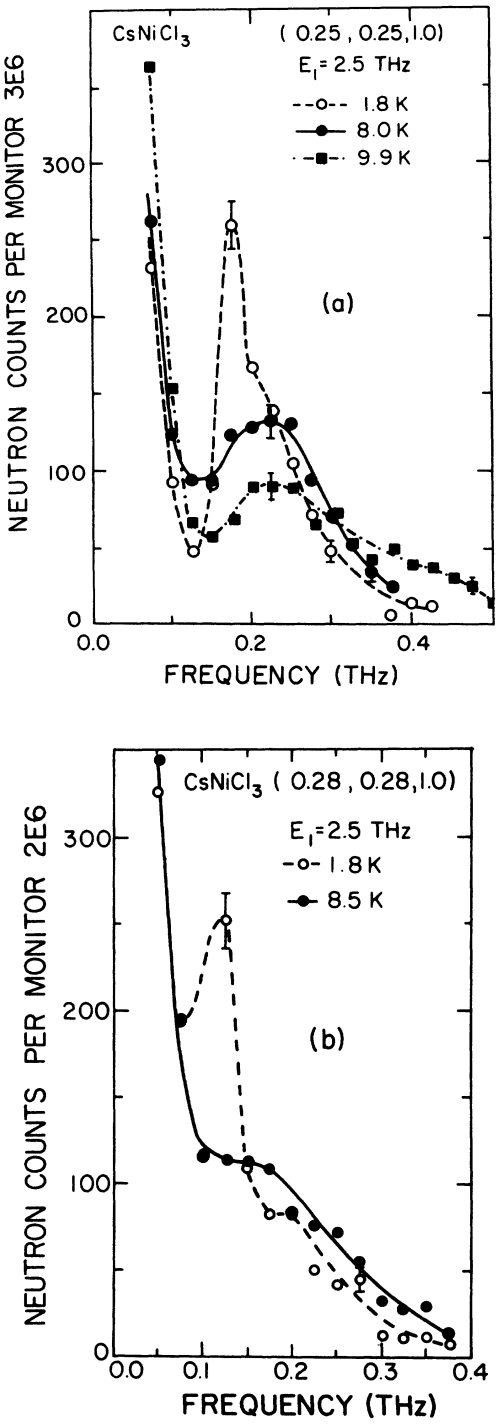

FIG. 13. Constant-Q scans at (a) (0.25,0.25,1) and (b) (0.28,0.28,1) at several temperatures.

as shown by Scalapino, Imry, and Pincus,[34] where $\mathbf{q}_b$ is the wave-vector component in the basal plane. The spin-wave frequencies along $\mathbf{Q}(\eta,\eta,1)$, where $\mathbf{q}_b=(\eta,\eta,0)2\pi/a$, are

$$\nu^2(\mathbf{q}_b)=\nu_0^2+A\tilde{J}'(\mathbf{q}_b)\ .$$

This equation, which gives a good fit to the measured dispersion (Fig. 15), is obtained with model parameters $A\tilde{J}'=0.028\pm0.005$ THz^2, $\nu_0=0.32\pm0.03$ THz. Our best estimate, therefore, of the gap frequency of a single chain of Ni^{2+} ions in $CsNiCl_3$ is 0.32 THz, after account has been taken of the 3D effects.

These parameters are reasonable in that if A is taken from linear spin-wave theory to be $\sim 4JS$ then $\tilde{J}'$ turns out to be 0.009 ± 0.002 THz, comparable with the interchain coupling determined earlier at low temperature. Thus our model of a set of weakly coupled oscillators is substantiated. The existence of dispersion in the 1D phase therefore results from the presence of a finite resonance frequency for each isolated chain. If there were no gap the critical scattering would consist of a quasielastic peak whose width narrowed on approach to the $(\frac{1}{3},\frac{1}{3},1)$ ordering wave vector. The finite-gap frequency collects this critical scattering into the observed finite-frequency dispersive branch. Thus we would not expect to find strong quasielastic critical scattering if our interpretation is correct. Our measurements as a function of q_b confirm that any elastic critical scattering at $\eta=\frac{1}{3}$ and $\frac{2}{3}$ is very small. The presence of low-intensity quasielastic scattering was sought in scans along $(\eta,\eta,1)$ for $\nu=0$ at a resolution of 0.25 THz but little or none was found. Figure 16 shows the data collected at 10 K as compared to that at 3 K where strong elastic peaks at $\eta=\frac{1}{3}$, $\frac{2}{3}$, and $\frac{4}{3}$ are observed. For a frequency offset of $\nu=0.1$ THz, peaks were observed near $\eta=\frac{1}{3}$, $\frac{2}{3}$, and $\frac{4}{3}$ (Fig. 17) but their intensities were consistent with the edge of the resolution intersecting the well-defined inelastic peaks. Only as T approaches 4.4 K was quasielastic scattering observed as a soft mode develops at $(\frac{1}{3},\frac{1}{3},1)$.[35]

According to classical spin-wave theory, an anisotropy of $D=-0.037\pm0.007$ THz would be required to produce a gap of 0.32 ± 0.03 THz. Our measurements in the 3D phase, however, revealed that the anisotropy constant is $D=-0.013\pm0.002$ THz which is three times smaller than the value required. The zone-center frequency of an isolated chain is significantly larger than would be expected for a classical chain with the known small anisotropy.

An even stronger argument made independently by Steiner *et al.*[33] and Kadowaki, Ubukoshi, and Hirakawa[24] that the gap is not caused by single-ion anisotropy comes from the magnitude (1.92 T) of the spin-flop field[22] and the observed anisotropy of the susceptibility. The argument shows that this leads to a very small anisotropy parameter ($0>D>-0.0026$ THz). Thus $|D|$ as determined from the spin-flop field is five times smaller than $|D|$ determined from the spin-excitation spectrum. We suggest that the dynamic properties lead to an effective $|D|$ that is much larger than the bare $|D|$ because of the inclusion, even in the 3D phase, of

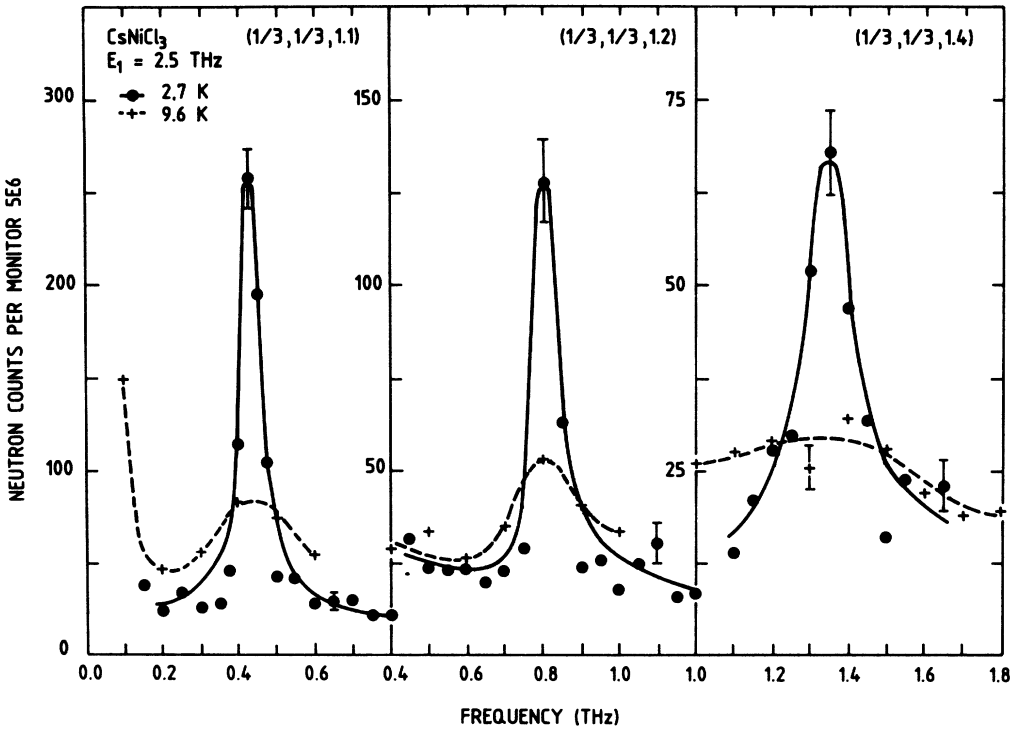

FIG. 14. Constant-Q scans at $(\frac{1}{3},\frac{1}{3},1+\eta)$ at 2.7 and 9.6 K.

some of the Haldane gap effect in the effective parameter $|D|$ of our linear spin-wave theory. The very low bare $|D|$ enhances our conclusion that the gap observed in the 1D phase arises from the Haldane effect.

These results show that $CsNiCl_3$ is indeed a very good approximation to the class of nearly Heisenberg systems for which a finite gap in the energy spectrum has been predicted. According to the most recent Lanzcös estimates by Parkinson *et al.*[10] the gap frequency is $0.40\times(2J)$ or 0.28 THz, while according to Botet, Jullien, and Kolb[4] it is $0.25\times(2J)=0.17$ THz. The first estimate lies close to the 0.32-THz frequency determined in this study of $CsNiCl_3$. Experiment, therefore, lends support to the Haldane conjecture that a gap exists in the spin-1 antiferromagnetic chain near the Heisenberg point. The

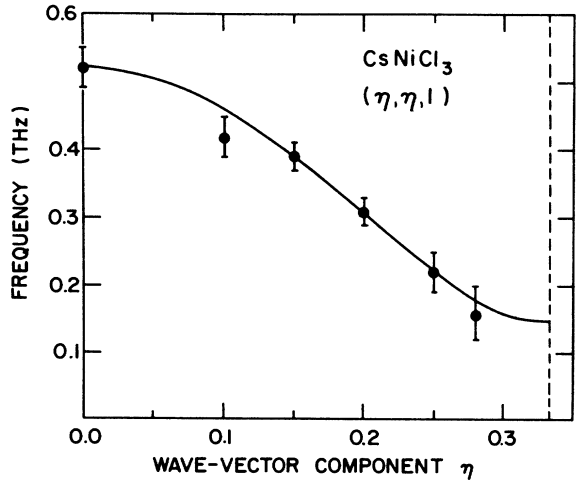

FIG. 15. Fit of spin-wave dispersion $\nu^2(q_b)=\nu_0^2+AJ'(q_b)$ with $\nu_0=0.32$ THz, $AJ'=0.028$ THz^2 to measured spin-wave peak frequencies along $(\eta,\eta,1)$ for temperatures in the range 7–10 K.

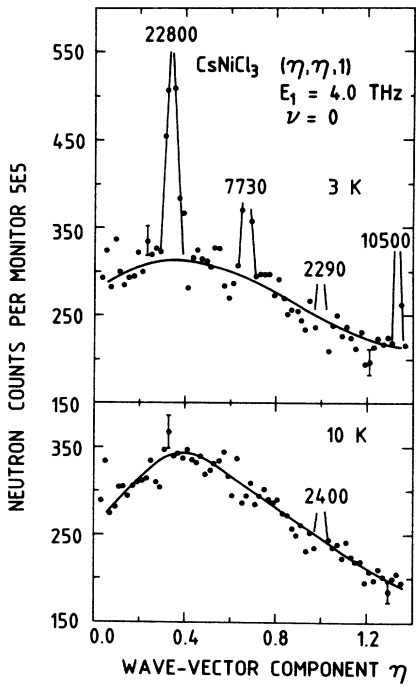

FIG. 16. Quasielastic scans along $(\eta,\eta,1)$ for energy transfer $\nu=0$ at 3 and 10 K.

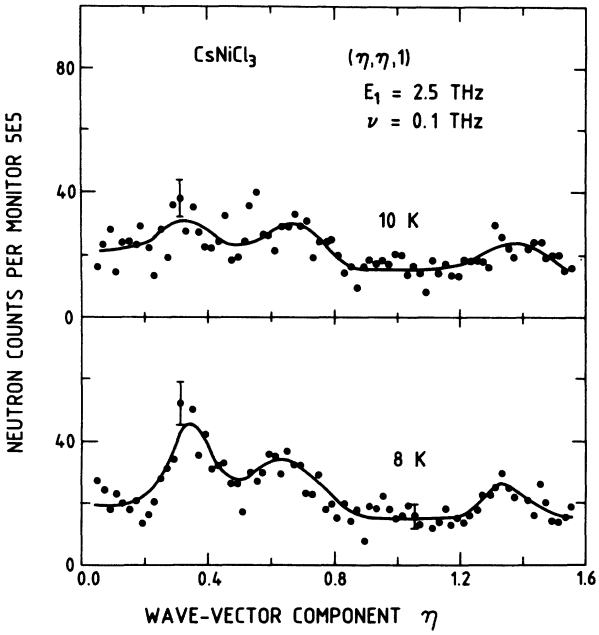

FIG. 17. Quasielastic scans along $(\eta,\eta,1)$ for energy transfer $\nu=0.1$ THz at 8 and 10 K.

comparison between the theoretical predictions and the present experimental result is illustrated schematically in Fig. 18.

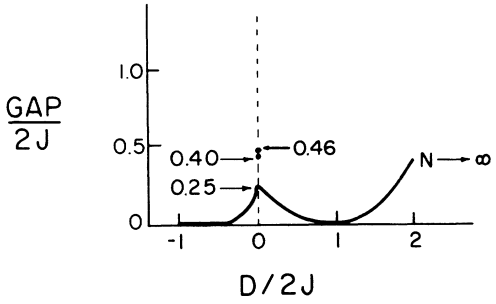

FIG. 18. Comparison between the theoretical predictions and the present experimental result. The gap of 0.46 corresponds to what was measured in the experiment; the other two values are the theoretical predictions (Refs. 4 and 10).

VI. SUMMARY OF RESULTS

The spin-wave spectrum, both frequencies and intensities, for the canted structure of the 3D ordered phase, has been calculated from the generalized spin susceptibility for an ordered magnetic system consisting of several sublattices. Spin-wave peaks have been measured by neutron scattering and fitted to the spin-wave model. The exchange and anisotropy parameters determined, namely, $J=0.345\pm0.008$ THz, $J'=0.0060\pm0.0005$ THz, and $D=-0.0130\pm0.0015$ THz, confirm that $CsNiCl_3$ is a good approximation to a 1D Heisenberg antiferromagnet.

The gap frequency 0.32 THz for an isolated chain of Ni^{2+} ions has been determined by neutron-scattering measurements above 4.8 K. The size of the gap cannot be explained by the small value for the anisotropy D determined from the 3D data either from the spin-wave data or *a posteriori* from the spin-flop field. The value is, however, consistent with recent calculations of the gap frequency for an isotropic spin-1 antiferromagnetic Heisenberg chain. The results of this study of the spin dynamics in $CsNiCl_3$ therefore support the Haldane conjecture that integer-spin chains have ground-state properties that are inherently different from those of half-integer–spin chains.

A ring of half-integer spins has different symmetry from a ring of integer spins as a result of time-reversal invariance. For every Ising component of a wave function there is an odd or even mixture of the time-reversed components. Thus for an even number of atoms the ground state of the $S=\frac{1}{2}$ system has odd parity with momentum $Q=\pi$, while that of the $S=1$ system has even parity with $Q=0$. This ties in with the presence of components having $S_i^z=0$ only in the ground state of the $S=1$ system. Since $Q=0$ does not break the symmetry a gap can persist to $T=0$ as shown by Affleck *et al.*[36]

Mattis[37] has also drawn attention to the $S_i^z=0$ components and suggested by a transformation $S'\rightarrow S+\frac{1}{2}$ that the integer-spin systems feel an effective uniform field that creates a Zeeman anisotropy in the antiferromagnet. However, the argument is only semiclassical, requires the addition by hand of extra states, and is inconsistent if the transformation is applied twice or for higher dimensional systems in the known large-spin limit.

Recently Affleck[38] on the basis of ideas related to those of Haldane has produced a series of mappings from two-dimensional classical continuum field theories to various types of quantum-spin chains, including systems with integer spin. The work leads to a number of predictions.[36,38–40] These developments confirm Haldane's conjecture and lead to suggestions for additional experiments.

ACKNOWLEDGMENTS

We are grateful to H. N. Nieman and D. C. Tennant for technical assistance and Zin Tun for help with the manuscript. We have benefited from discussions with J. K. Kjems, K. Kakurai, M. Steiner, I. Affleck, H. Kadowaki, and J. S. Rosenthal.

[1]F. D. M. Haldane, Phys. Rev. Lett. **50**, 1153 (1983).
[2]J. C. Bonner, J. Appl. Phys. **61**, 3941 (1987).
[3]R. Botet and R. Jullien, Phys. Rev. B **27**, 613 (1983).
[4]R. Botet, R. Jullien, and M. Kolb, Phys. Rev. B **28**, 3914 (1983).
[5]D. C. Mattis, Phys. Rev. B **31**, 4698 (1985).
[6]J. Sólyom and T. A. L. Ziman, Phys. Rev. B **30**, 3980 (1984).
[7]J. C. Bonner and G. Muller, Phys. Rev. B **29**, 5216 (1984).

[8]R. Botet, R. Jullien, and M. Kolb, Phys. Rev. B **29**, 5222 (1984).
[9]M. Kolb, R. Botet, and R. Jullien, J. Phys. A **16**, L673 (1983).
[10]J. B. Parkinson, J. C. Bonner, G. Muller, M. P. Nightingale, and H. W. L. Blote, J. Appl. Phys. **57**, 3319 (1985).
[11]W. J. L. Buyers, R. M. Morra, R. L. Armstrong, M. J. Hogan, P. Gerlach, and K. Hirakawa, Phys. Rev. Lett. **56**, 371 (1986).
[12]J. P. Renard, M. Verdaguer, L. P. Regnault, W. A. C. Erkelens, J. Rossat-Mignod, and W. G. Stirling, Europhys. Lett. **3**, 945 (1987).
[13]W. J. L. Buyers, Trans. R. Soc. Can. Sect. 5 **1**, 241 (1986).
[14]N. Achiwa, J. Phys. Soc. Jpn. **27**, 561 (1969).
[15]D. Moses, H. Shechter, E. Ehrenfreund, and J. Makovsky, J. Phys. C **10**, 433 (1977).
[16]D. P. Almond, Physica **86-88B**, 651 (1977).
[17]Y. Barjhoux, J.-P. Boucher, and J. Karra, Physica **86-88B**, 1307 (1977).
[18]K. R. Mountfield and J. A. Rayne, J. Phys. (Paris) **42**, 468 (1981).
[19]P. A. Montano, E. Cohen, and H. Shechter, Phys. Rev. B **6**, 1053 (1972).
[20]A. Sorgen, E. Cohen, and J. Makovsky, Phys. Rev. B **10**, 4643 (1974).
[21]P. B. Johnson, J. A. Rayne, and S. A. Friedberg, J. Appl. Phys. **501**, 1853 (1979).
[22]E. Cohen and M. D. Sturge, Solid State Commun. **24**, 51 (1977).
[23]R. H. Clark and W. G. Moulton, Phys. Rev. B **5**, 788 (1972).
[24]H. Kadowaki, K. Ubukoshi, and K. Hirakawa, J. Phys. Soc. Jpn. **56**, 751 (1987).
[25]V. J. Minkiewicz, D. E. Cox, and G. Shirane, Solid State Commun. **8**, 1001 (1970).
[26]D. E. Cox and V. J. Minkiewicz, Phys. Rev. B **4**, 2209 (1971).
[27]W. B. Yelon and D. E. Cox, Phys. Rev. B **7**, 2024 (1973).
[28]J. A. Rayne, J. G. Collins, and G. K. White, Solid State Commun. **33**, 39 (1980).
[29]B. B. Garrett and W. B. Euler, Solid State Commun. **28**, 505 (1978).
[30]W. J. L. Buyers, T. M. Holden, and A. Perreault, Phys. Rev. B **11**, 266 (1975).
[31]R. Feile, J. K. Kjems, A. Hauser, H. U. Gudel, U. Falk, and A. Furrer, Solid State Commun. **50**, 435 (1984).
[32]Xiaodong Zhu and M. B. Walker, Phys. Rev. B **36**, 3830 (1987).
[33]M. Steiner, K. Kakurai, J. K. Kjems, D. Petitgrand, and R. Pynn, J. Appl. Phys. **61**, 3953 (1987).
[34]D. J. Scalapino, Y. Imry, and P. Pincus, Phys. Rev. B **11**, 2042 (1975).
[35]D. Petitgrand, M. Steiner, and J. K. Kjems, Risø National Laboratory Report No. Riso-R-517, 13, 1985 (unpublished).
[36]I. Affleck, T. Kennedy, E. H. Lieb, and H. Tasaki, Phys. Rev. Lett. **59**, 799 (1987).
[37]D. C. Mattis (unpublished).
[38]I. Affleck, Nucl. Phys. **B265**, 409 (1986).
[39]I. Affleck, Phys. Rev. Lett. **56**, 408 (1986).
[40]I. Affleck, Phys. Rev. Lett. **57**, 1048 (1986).